Scroll wave filaments self-wrap around unexcitable heterogeneities

Zulma A. Jiménez and Oliver Steinbock

Department of Chemistry and Biochemistry, Florida State University, Tallahassee, Florida 32306-4390, USA

Scroll waves are three-dimensional excitation vortices rotating around one-dimensional phase singularities called filaments. In experiments with a chemical reaction-diffusion system and in numerical simulations, we study the pinning of closed filament loops to inert cylindrical heterogeneities. We show that the filament wraps itself around the heterogeneity and thus avoids contraction and annihilation. This entwining steadily increases the total length of the pinned filament and reshapes the entire rotation backbone of the vortex. Self-pinning is fastest for thin cylinders with radii not much larger than the core of the unpinned rotor. The process ends when the filament is attached to the entire length of the cylinder. The possible importance of self-pinning in cardiac systems is discussed.

I. INTRODUCTION

Dynamic diseases are a widely uncharted area of modern science, partly because their fundamental origins are not molecular, cellular, or tissue abnormalities but rather undesired dynamic states of complex networks [1]. Important examples are the occurrence of epileptic seizures and certain cardiac arrhythmia. A seizure, for instance, involves an enormously large number of synchronized neurons [2]. Tachycardia and the reentry of electrical activity in the heart, on the other hand, correspond to spatiotemporal patterns that involve rotation around a phase singularity [3]. Numerous studies have discussed the close link between rotating waves in cardiac tissue and nonbiological reaction-diffusion systems such as the Belousov-Zhabotinsky (BZ) reaction [4,5]. The latter reaction is a spatially homogeneous and isotropic, active medium. In two space dimensions, it self-organizes rotating spiral waves of typically constant pitch. The spiral tip describes a trajectory that in the simplest case is a circular orbit with a diameter much smaller than the pattern wavelength.

It is widely accepted that two-dimensional models are insufficient to describe ventricular tachycardia and, in particular, ventricular fibrillation [6,7]. Rotation in three-dimensional systems, however, cannot occur around a pointlike phase singularity but must rather be organized around one-dimensional curves. These curves are commonly referred to as filaments while their surrounding wave fields are called scroll waves [8–10]. Filaments are dynamic objects and move with local speeds that—to some approximation—are proportional to the local curvature κ [11]. Theoretical analyses [11,12] of reaction-diffusion models yield the equation

$$\frac{d\mathbf{s}}{dt} = (\alpha\hat{\mathbf{N}} + \beta\hat{\mathbf{B}})\kappa, \qquad (1)$$

where t is time, $\mathbf{s}$ is a position vector pointing to a location on the filament, and $\hat{\mathbf{N}}$ and $\hat{\mathbf{B}}$ are the corresponding normal and binormal unit vectors, respectively. The proportionality constants α and β are system-specific parameters which depend, in a nontrivial fashion, on the underlying rate constants and diffusion coefficients. The parameter α plays the role of a filament tension. For positive values of α, filament loops collapse and annihilate in finite times [9,13]; negative values induce chaotic motion known as Winfree turbulence

[14,15]. This form of spatiotemporal chaos exists only in three-dimensional media and has been linked to ventricular fibrillation [16,17]. The parameter β controls motion in binormal direction that for a planar loop coincides with an out-of-plane translation. In activator-inhibitor systems with equal diffusion coefficients and in the complex Ginzburg-Landau equation, the value of β is zero [18].

Excitation vortices can pin to stationary as well as slowly moving heterogeneities [19,20]. A simple example is the pinning of two-dimensional spirals to small, static heterogeneities that are permeable but unexcitable. This basic form of vortex pinning has been studied in chemical reactions [21], aggregating slime molds [22], the CO oxidation on platinum surfaces [23], and cardiac tissue as well as cardiac cell cultures [24]. The pinning of three-dimensional excitation vortices was demonstrated experimentally by our group in 2009 [25]. Since then we have reported examples of scroll wave pinning to inert and impermeable tori, double tori, as well as single and multiple spheres [26–28]. These studies show that pinning can increase the lifetime of collapsing scroll waves ($\alpha > 0$) and even establish stationary filaments. We also reported that heterogeneities can create local differences in the rotation period that twist the emitted wave field. The dynamics of this process and the opposing response of the nonlinear reaction-diffusion system are described by the forced Burgers equation [25,29]. In addition, Pertsov *et al.* established topological constraints that govern the pinning of multiple filaments to a given heterogeneity [30]. These laws state that the sum of all topological charges, an integer quantity defined by the sense of rotation, must add up to zero on any given closed surface. As a consequence, the total number of filaments pinned to a given heterogeneity is always even.

In this article we investigate the fate of scroll waves that are partially pinned to cylindrical heterogeneities. We find that a single contact point between the filament and the heterogeneity is sufficient to induce a process that ultimately incorporates the entire cylinder into the rotation backbone of the scroll wave. This self-pinning stabilizes and reshapes the vortex pattern. In the context of the human heart such vortex pinning and reshaping could be induced by blood vessels and scar tissue (structurally remodeled myocardium) from infarcts and other traumatic events. The core region of such tissue can be nonconducting [31,32] and might hence

be a suitable "anchor" for rotating action potentials. One can further speculate that such pinning will reduce the efficiency of low-power intervention techniques [33] such as implantable cardioverter defibrillators. The systematic investigation of such phenomena is therefore of great interest, both from a fundamental and an applied, biomedical perspective.

II. EXPERIMENTAL METHODS

For our experiments, we use the ferroin-catalyzed Belousov-Zhabotinsky (BZ) reaction. This autocatalytic reaction is a well-known model for the study of spiral and scroll waves in excitable and oscillatory reaction-diffusion systems [8,9,13,34]. The system consists of a lower gel layer (0.8% w/v agar) and a top liquid layer [25]. Both layers are 4 mm thick and contain a reaction medium of essentially identical concentrations. Disregarding the bromination of malonic acid, the initial concentrations are $[NaBrO_3] = 0.04$ mol/L, [malonic acid] $= 0.04$ mol/L, $[H_2SO_4] = 0.16$ mol/L, and $[Fe(phen)_3SO_4] = 0.5$ mmol/L. In addition, all diffusion coefficients are expected to be identical throughout the two-layer system. From the collapse of unpinned scroll rings, we find the filament tension in this system to be $\alpha = (1.4 \pm 0.2) \times 10^{-5}$ cm^2/s. For the given layer height, a centered scroll ring evolves without measurable boundary effects. Smaller heights or closer proximities to the system boundaries, however, are expected to influence the dynamics of the scroll wave. Moreover, earlier studies have shown that the parameter β [see Eq. (1)] is approximately zero [25]. For filaments with low curvature and twist, free filament motion in binormal direction is hence negligible.

During the gelation process, we place cylindrical glass rods onto the gel surface and gently press them halfway into the forming gel. After completion of gelation, we add the liquid layer and initiate a nonrotating, nearly spherical chemical wave using the tip of a silver wire. The chemical mechanism behind the Ag-mediated wave nucleation is the formation of insoluble AgBr which decreases the local concentration of inhibitory bromide ion. The system is then manually swirled to create a homogeneous, excitable upper layer. Notice that this motion does not affect the expansion of the half-spherical wave in the gel. Once the wave reaches the desired size (typically the size needed to be in contact with the cylindrical heterogeneity), we stop the mechanical agitation and all fluid flow ceases. At this time we also place a flat glass plate onto the system to prevent fluid-dynamic perturbations that could arise from undesired processes in the liquid layer and at the liquid-air interface. Notice that the height of the liquid layer remains essentially constant at 4 mm. Subsequently, the rim of the half-spherical wave curls up into the top layer and nucleates a scroll ring (see the Supplemental Material [35] for a schematic view of the procedure described here). In a typical experiment, its nearly circular filament is pinned to the heterogeneity in at least one position.

The subsequent evolution of the wave patterns is monitored with a CCD camera equipped with a dichroic blue filter. The camera is mounted over the BZ system and the local intensity in each image pixel is hence a measure of the transmitted light across the 8 mm thick layer at that specific location. Image contrast results from the absorption of light by the chemically reduced catalyst. Wave patterns can be observed for more than 6 h. All experiments are carried out at 21.5 °C.

III. EXPERIMENTAL RESULTS

Figure 1(a) shows a snapshot of a typical experiment recorded a few seconds after termination of the mechanically sustained mixing of the top layer. This instant corresponds to the nucleation of the scroll wave from the bowl-shaped wave in the gel layer. Bright and dark regions indicate primarily excited and excitable areas, respectively. We reemphasize that the local gray levels are the result of light absorption along a line of spatially variable concentration of the absorbing catalyst species. The bright, rectangular region near the middle of the image frame is the cylindrical glass object, which in this experiment has a length of 12 mm and a radius of 1.0 mm. Notice that the rim of the excitation wave touches the cylinder. Figure 1(b) shows the same system approximately 2 h later. Despite the positive filament tension in this BZ system, the scroll wave has not collapsed but organizes a kidney-shaped, periodic wave pattern.

For the given perspective, the filament of the scroll wave appears as a curve that emits waves to both of its sides in an alternating fashion. Clearly this cyclic wave generation is due to the—spatially not fully resolved—rotation in three dimensions. Closer inspection of the dynamics reveals that the filament in Fig. 1(b) traces approximately the bright, diffuse wave border that connects the end points of the pinning cylinder. Figure 1(c) shows the result of a quantitative analysis of the filament position. This computerized analysis detects the filament (or more precisely its two-dimensional projection) as a set of image pixels that show only small intensity changes during one approximate rotation period of the pattern. A similar method was first used by Vinson *et al.* [9].
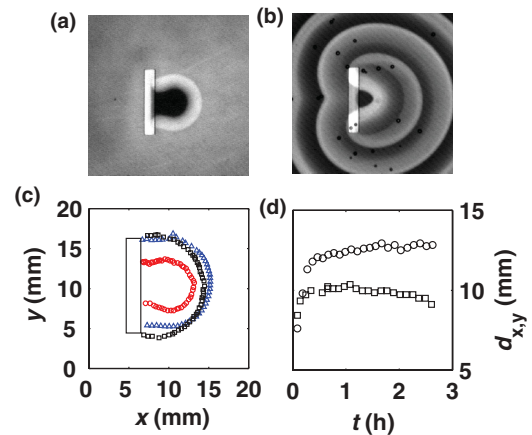

FIG. 1. (Color online) (a), (b) View through a 8 mm thick BZ system in which a scroll wave (grayish pattern) is pinned to a glass cylinder (bright rectangle; height 12 mm; radius 1 mm). Frame (a) has been recorded immediately after the initiation of the scroll wave, frame (b) 116 min later. Image area: 29×29 mm^2. (c) Filament positions in the same experiment approximately 0 min (red, innermost curve), 8 min (blue triangles), and 196 min (black squares) after initiation. (d) Temporal evolution of the maximal distance d_x between the filament and the cylinder (squares) and the maximal extension d_y of the filament along the cylinder axis (circles).

The data in Fig. 1(c) reveal that the initially small filament loop (red circles) expands quickly to a seemingly stationary, C-shaped structure. The filament terminates at the cylinder in nearly normal direction. Notice that wave rotation occurs also around the cylinder itself, which connects the overall rotation backbone topologically to a closed loop. The rotation around the cylinder has a lower frequency than the freely rotating filament because the cylinder perimeter is larger than the free spiral core orbit. This frequency difference induces twist along the cylinder axis, which can be discerned in Fig. 1(b). It is probably also responsible for the kidney shape of the emitted wave fronts.

Figure 1(d) shows the temporal evolution of the maximal distance d_x between the free filament and the cylinder (squares) and the maximal extension d_y of the free filament in the direction parallel to the cylinder (circles). The data reveal an initial, rapid increase in both measures, which could be partly caused by our specific initiation method. Subsequently both distances change only slowly. More specifically, we observe a slight increase in d_y and a slight decrease in d_x. These slow dynamics must be compared to the motion of free scroll rings in this system, which have a life time of $t_L = R_0^2/(2\alpha)$ (see, e.g., Ref. [25]). For the given filament tension and an initial radius of $R_0 = 5$ mm, the free vortex annihilates within 2.5 h. This comparison shows that pinning to a single, cylindrical heterogeneity can prevent, or at least greatly delay, the collapse and the self-annihilation of scroll rings. We also note that further observation of the wave structure in Fig. 1 was possible for a total of 7 h during which the vortex remained intact. However, the closed BZ system undergoes chemical changes that are most pronounced in its late stages. These changes alter wave speed, rotation frequency, and possibly filament tension. Consequently, we did not include these data in the figure.

One would expect that the motion of the contact points between the free filament and the cylinder is affected by the shape of the unpinned filament. We hence investigated other configurations such as the one in Fig. 2. Figures 2(a) and 2(b) show an early and late view of a scroll wave pinned to two glass rods that we arranged side by side at a distance of 8.1 mm. The length and radius of these unexcitable cylinders are 14 and 1.0 mm, respectively. The time elapsed between the two frames is 174 min. The small circular objects in Fig. 2(b) are gas bubbles that nucleate and grow due to the formation of CO_2 in the BZ reaction. The image shows that the filament loop connects to both glass rods, which again prevents the filament-tension-induced collapse of the vortex structure.

Figure 2(d) is a time-space plot which is constructed by collecting subsequent image profiles and stacking them in a downward direction. In this case, the intensity profiles are obtained along the centerline between the two cylinders [vertical in Figs. 2(a) and 2(b)]. In the time-space plot this space axis is oriented horizontally and time evolves in a downward direction spanning 3 h. Each white band corresponds to a propagating wave front. The intersections between the profile line and the two filaments arches appear as wave emitting points. Figure 2(c) shows the temporal evolution of the distance d_y between these two points, which increases over time. The overshoot around 0.5 h is an unusual feature, which we tentatively explain by the formation of twist.
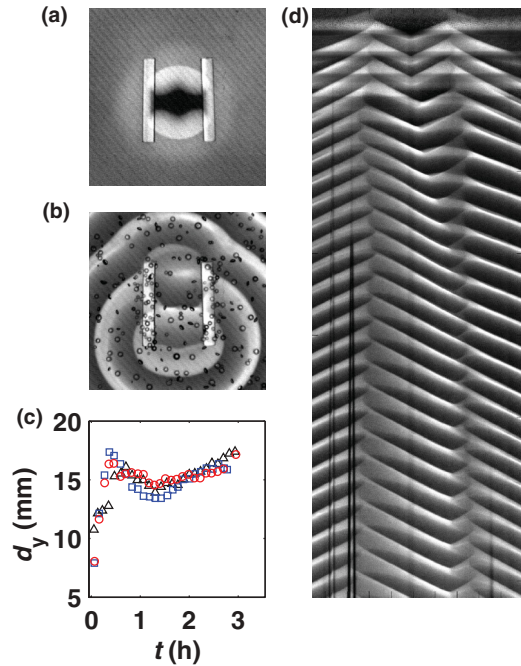

FIG. 2. (Color online) (a), (b) View through a three-dimensional BZ system in which a scroll wave is pinned to two glass cylinders with an individual length of 14 mm and a radius of 1 mm. Frame (a) has been recorded immediately after the initiation of the scroll wave, frame (b) 174 min later. Image area: 30×30 mm². (c) Distance between the upper and the lower filament segments as a function of time. The distance is measured close to the right edge of the left cylinder (red circles), close to the left edge of the right cylinder (blue squares), and in their middle (black triangles). (d) Time-space plot constructed along the vertical line in (a), (b) that has equal distance to the two cylinders. Time evolves in downward direction and spans 3 h.

The final vortex structure is nearly stationary with free filament segments connecting the neighboring end points of the two cylindrical heterogeneities. Their maximal distance (approximately 17 mm) is slightly larger than the length of the pinning glass rods (14 mm). The free segments periodically emit inward and outward propagating waves that collide in the central region between the two cylinders. In the time-space plot, these collisions create V-shaped features that are clearly not centered between the wave emitting points. This asymmetry was observed in several experiments but its origin is not completely understood.

The experiments shown in Figs. 1 and 2 raise the important question whether the filament loop would expand further if pinned to a single, longer cylindrical heterogeneity. However, for such situations we observe the buildup of strong twist that tilts the filament out of its initial plane and typically induces filament collisions with the system boundary. The resulting patterns appear to be rather complicated and have not been analyzed further.

An alternative approach is illustrated in Fig. 3. This experiment employs two long cylinders arranged on a common line. The gap between the cylinders is 8.5 mm wide. Using the protocol described above, we initiate a scroll ring in the middle of this gap and ensure that its filament is in contact with both
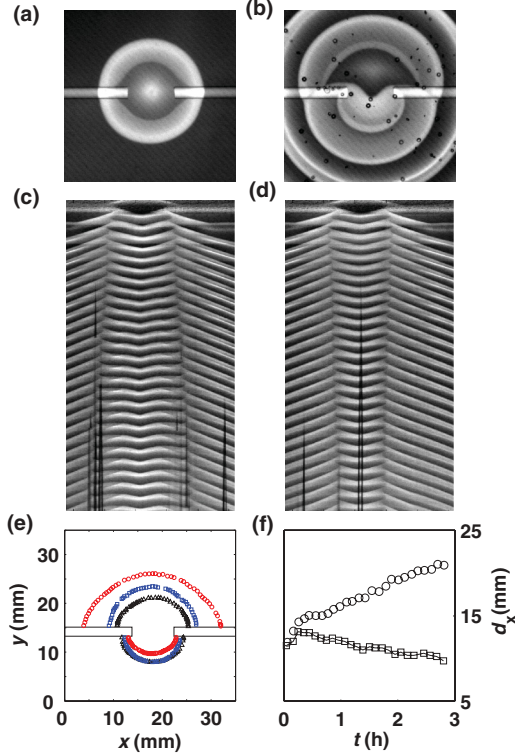
FIG. 3. (Color online) (a), (b) View through a three-dimensional BZ system in which a scroll wave is pinned to two glass cylinders with an individual length of 14 mm and a radius of 1 mm. Frame (a) has been recorded immediately after the initiation of the scroll wave, frame (b) 116 min later. Image area: 32×32 mm^2. (c), (d) Time-space plots constructed along vertical lines slightly above (c) and below (d) the cylinders shown in (a), (b). Time evolves in downward direction and spans 3 h. (e) Reconstructed filaments at 16 min (black triangles), 76 min (blue squares), and 256 min (red circles). (f) Temporal evolution of the width of the upper (circles) and lower (squares) filament arches.

cylinders [Fig. 8(a)]. Notice that the early filament connects to the cylinder not tangentially as in Figs. 1 and 2 but rather in a normal direction. Figure 3(b) shows the pinned vortex about 2 h after the recording of Fig. 3(a). The vortex is still present but the wave structure has clearly lost its symmetry with respect to the cylinder-connecting axis.

The dynamics that give rise to this profound change are illustrated in the time-space plots shown in Figs. 3(c) and 3(d). Referring to the images in Figs. 3(a) and 3(b), the intensity profiles are collected along a horizontal line slightly above the cylinders [Fig. 3(c)] and a parallel line slightly below the cylinders [Fig. 3(d)]. Both figures show two wave emitting points which correspond to the filament intersections. The distance between these points increases in Fig. 3(a) and decreases in Fig. 3(b) and is further characterized in Fig. 3(f). The entire dynamics of this process, however, is not limited to the motion of the contact points between filament and obstacle but also involve the connecting filament arches in the upper and lower image halves. Their shapes are plotted in Fig. 3(e) for three different times. About 16 min after scroll initiation (black triangles), the two filament arches still form a nearly continuous circle. One hour later (blue squares),

the small mismatch between the arches in the x direction has significantly increased and the upper filament has also expanded in the y direction. At 256 min (red circles), the upper filament has expanded further while the lower one has moved slightly towards the cylinder-connecting line. One can speculate that the shrinking filament arch will eventually connect the gap between the cylinders as a nearly straight line as such a shape would result from the system's free curvature flow [see Eq. (1)].

The observed dynamics show several phenomena which can be summarized as follows: (i) Filaments terminating at cylindrical (inert and impermeable) heterogeneities can move along the cylinder axis; (ii) this motion stops at the end of the cylinder; (iii) the connecting free filament arches can expand or shrink depending on the relative direction of their termination points (as well as their own curvature); and (iv) the expansion of the free filament segments occurs despite their concave shape, which should generate an opposite motion. Another key observation relates to the drift direction of the pinned filaments. Based on the available experimental data, the governing principle is the increase in the length of the pinned of filament.

The self-wrapping of scroll waves around unexcitable heterogeneities is a feature that should have profound consequences on the stability, dynamics, and persistence of scroll wave in heterogeneous excitable systems. It also raises the perplexing question as to how a vortex responds if the initial situation is perfectly symmetric. The experiment in Fig. 3 is a good approximation of such a case and one can wonder why filament expansion and shrinkage did not occur in the opposite image halves. Repeat runs of this particular experimental configuration show that both scenarios are possible. This issue will be revisited in the context of the numerical simulations in Figs. 8 and 9.

IV. COMPUTATIONAL METHODS

To obtain further insights into the self-pinning of filaments, we have performed numerical simulations on the basis of the Barkley model [36]. This reaction-diffusion model involves two variables u and v that obey

$$\frac{\partial u}{\partial t} = \nabla^2 u + \frac{1}{\epsilon} u (1-u) \left(u - \frac{v+b}{a} \right), \qquad (2)$$

$$\frac{\partial v}{\partial t} = \nabla^2 v + u - v. \qquad (3)$$

In our simulations the model parameters are $\epsilon = 0.02, a = 1.1$, and $b = 0.18$. These values yield excitable point dynamics and define a medium in which spiral waves have circular tip trajectories. In spatially three-dimensional systems, they cause positive filament tension ($\alpha > 0$) [18]. Since the diffusion coefficients of u and v are identical (here equaling one), free filaments of low curvature and twist show no translation in the binormal direction ($\beta = 0$) [18].

Equations (2) and (3) are integrated using explicit Euler integration, a seven-point stencil for the Laplacian, a three-dimensional lattice measuring $400 \times 400 \times 200$ grid points ($200 \times 200 \times 100$ grid points for the data in Figs. 8 and 9), and Neumann boundaries. The grid spacing and the integration time step are kept constant at 0.2 and 0.006, respectively. The pinning cylinders are modeled as regions where $u = v = 0$,
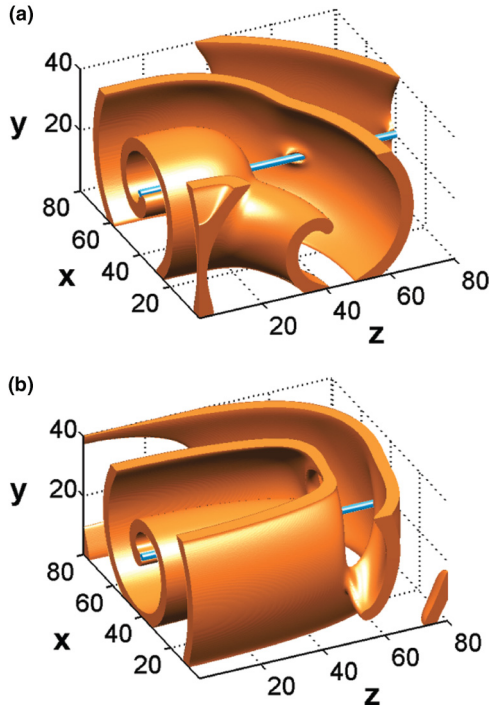
FIG. 4. (Color online) Snapshots illustrating the evolution of a self-wrapping scroll wave. Solid (orange) regions are in an excited state which corresponds to high values of the activator variable u. The unexcitable cylinder (cyan) extends in z-direction and has a radius of 1.0. Notice the increasing length of the pinned scroll wave. The time elapsed between frames is 205 time units, which corresponds to approximately 23 rotation periods.

which creates a Dirichlet boundary between the cylinder and the surrounding system. The filament is computed from the intersection of the waves' $u = 0.5$ and $v = a/2 - b$ surfaces using a marching-cube algorithm [37]. We initiate scroll waves from appropriately set initial conditions. For instance, the simulation in Fig. 4 uses $u = 0.25$ within a $90°$-disk segment of radius 40 centered around $(x,y) = 0$. The width of this excitable layer is 4.0 ($16 \leqslant z \leqslant 20$). To enforce the unidirectional propagation needed for vortex nucleation, we initially also inhibit the lower half of the system ($z < 16$) by initializing v as 0.4. All other points are initialized as $(u,v) = (0,0)$.

V. COMPUTATIONAL RESULTS

Figure 4 shows two snapshots of the wave field $u(x,y,z)$ for a scroll wave pinned to a cylindrical heterogeneity that extends along the entire system length in the z direction. Regions in which u has large values are rendered as solid (orange) areas and indicate that the system is locally excited. The initial condition of this simulation (not shown) establishes a filament tracing a quarter of a circle from the left end of the cylinder [$(x,y,z) = (50,20,0)$] to the anterior wall. The corresponding partial scroll ring is therefore in local contact with the unexcitable heterogeneity. The wave field shown in Fig. 4(a) is taken a few rotation periods after initiation but still shows the expected, doughnutlike shape in the posterior, left corner. Approximately 23 rotation periods later, the vortex
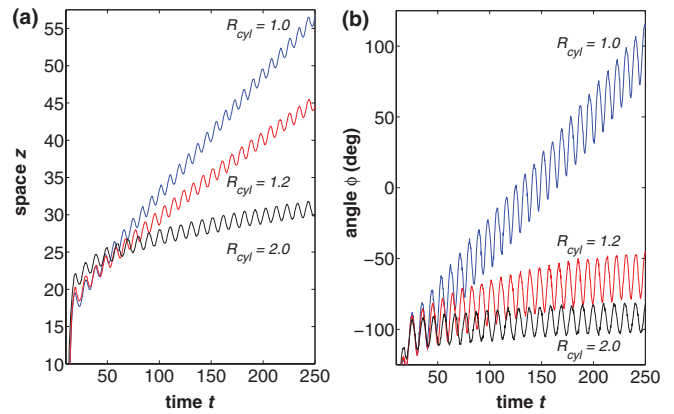

FIG. 5. (Color online) Filament movement along the pinning cylinder for cylinder radii of 1.0 (blue), 1.2 (red), and 2.0 (black). The time traces describe the motion of the end point of the free filament near the pinning cylinder. Using cylindrical coordinates (r,ϕ,z), (a) illustrates motion along the cylinder axis and (b) characterizes rotation around the cylinder. In all three cases, the extent of pinning increases over time.

structure has undergone profound changes. The dominant feature is now a nearly untwisted scroll wave that is pinned to the cylinder. At around $z = 60$ [Fig. 4(b)], this pattern ends rather abruptly and a defectlike vortex structure connects the filament to the anterior wall.

Clearly the simulation in Fig. 4 is in good agreement with the experimentally observed self-wrapping of scroll waves to unexcitable, cylindrical heterogeneities. Its geometry is a particularly good match for the experiment shown in Fig. 2 because the no-flux boundaries in the simulation can be interpreted as mirror planes for the computed concentration fields. Accordingly, the anterior wall in Fig. 4 ($x = 0$) can be thought of as a mirror plane generating an identical cylinder centered around $(x,y) = (-50,20)$. Similarly, the left wall ($z = 0$) mirrors the wave field in the $-z$ direction, thus completing the partial scroll ring to a full one.

Figure 5 provides additional information regarding the self-wrapping dynamics shown in Fig. 4. Here we follow the location of a particular point on the filament to monitor the progress of the self-pinning process. This point is defined in cylindrical coordinates (r,ϕ,z) as a filament position in close vicinity to the cylinder surface (the distance is $\Delta r = 2.0$). Figure 5(a) shows the z coordinate of this contact point for three different cylinder radii R_{cyl}. All three graphs increase over time while the average slope decreases with increasing values of R_{cyl}. The small oscillations on each graph are due to the intrinsic rotation of the vortex structure. Figure 5(b) describes the movement of the contact point in terms of its ϕ coordinate. Notice that increasing ϕ values indicate rotation around the cylinder perimeter. This rotation is most pronounced for $R_{\text{cyl}} = 1$ but still relatively slow as the point travels only $180°$ during the course of more than 26 rotation cycles of the scroll wave. The combined data in Fig. 5 show that the contact point moves along the cylinder on a stretched-out helical trajectory. For large radii this motion becomes negligible or is absent. This finding prompted us to repeat some of our experiments with glass rods of larger radii and we indeed failed to observe any significant amount
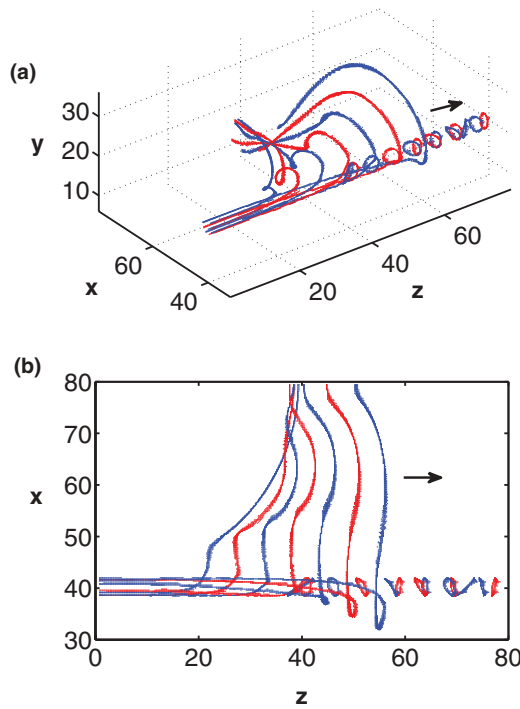
FIG. 6. (Color online) Filament evolution for the partially pinned scroll wave shown in Fig. 4(a) Three-dimensional data; (b) projection into the $(x,z$-plane). The pinning, unexcitable cylinder ($R = 1.0$, not shown) extends in z-direction. The black arrows indicate the principal direction of filament motion. The time interval between subsequent filament pairs is 35.5 time units. Alternating red and blue colors are used as a visual aid.
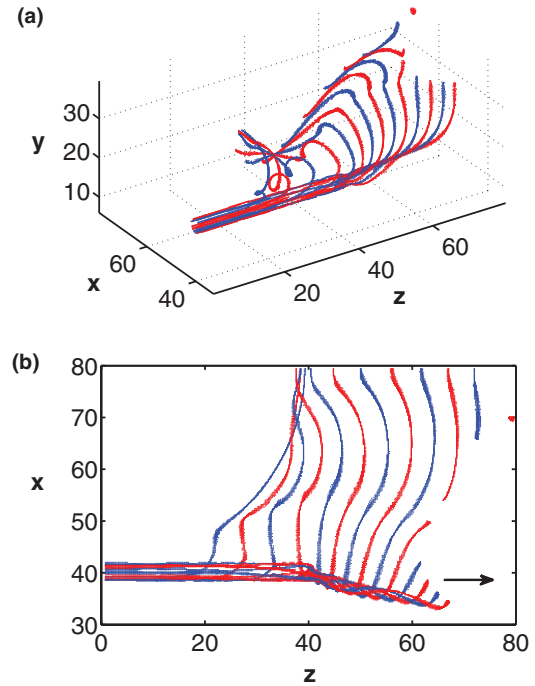

FIG. 7. (Color online) Filament movement along a pinning cylinder (not shown) of radius 1.0. The cylinder length equals only half the system length ($0 \leqslant z \leqslant 40$). The black arrow indicates the principal direction of filament motion. The time interval between subsequent filament pairs is 35.5 time units. Alternating red and blue colors are used as a visual aid.

of self-wrapping for $R_{cyl} = 1.5$ mm (see the Supplemental Material [35]).

An illustration of the motion of the entire self-wrapping filament is given in Fig. 6. The filaments are extracted from the simulation in Fig. 4. Figures 6(a) and 6(b) show the same three-dimensional data from two different viewpoints. The small circular loops for $z > 40$ stem from wave fronts punctured by the unexcitable cylinder. There is no rotation associated with these curves but for the given Dirichlet boundaries they are reliably detected by our algorithm and have hence been included. In addition, these loops are generated in collisions between the rotating, cylinder-bound filament and its free continuation. More importantly, Fig. 6(a) shows that the helical motion of the contact point is part of a large-scale deformation of the filament, which involves an extension in the forward direction and a continuous out-of-plane deformation of the free filament segment. The latter process can induce collisions of the filament with the outer system boundary, which obviously affect the subsequent dynamics significantly. Such collisions have also been observed in some of our BZ experiments (not shown).

Figure 7 describes the dynamics of self-wrapping filaments close to the end of the pinning cylinder. The diagrams have been arranged similarly to Fig. 6; here, however, the unexcitable cylinder extends only halfway through the system (namely, from $z = 0$ to $z = 40$). Initially the filament extends in a nearly perpendicular direction away from the

heterogeneity towards the wall. However, once the end of the cylinder is reached, the filament decreases its angle to the cylinder axis sharply and the resulting curves nearly extend in the z direction. We interpret this motion as a curvature-driven process that aims to smoothen the sharp filament kink produced during self-wrapping. Also notice that in this longer simulation, the filament collides with the upper system boundary. This collision shortens the filament which seemingly assists the straightening process of the filament.

Lastly we return to the questions of directionality and symmetry breaking. In contrast to experiments, numerical simulations allow us to study initial conditions that readily probe these important aspects of self-wrapping filaments. Figure 8 shows the evolution of three, only slightly different, initial conditions that—in the absence of heterogeneities— would create untwisted scroll waves with linear filaments spanning the system in the x direction. The angle between the initial filament and the cylinder axis is $(84.3)°$ in Figs. 8(a), 8(d), and 8(g), $(90.0)°$ in Figs. 8(b), 8(e), and 8(h), and $(95.7)°$ in Figs. 8(c), 8(f), and 8(i). The first row [Figs. 8(a)–8(c)] shows the u pattern shortly after initiation of the vortex. Over 300 time units these initial conditions evolve to the scroll waves shown in the next row [Figs. 8(d)–8(f)]. Notice the vortex in Fig. 8(e) has not changed significantly as it is still pinned to the same position of the cylindrical heterogeneity. As expected for a noise-free system, it also conserved its symmetry with respect to the $x = 20$ plane. Furthermore, the scroll wave is slightly twisted as the rotation close to the cylinder is slightly ahead of the remaining vortex. We suggest that this minor
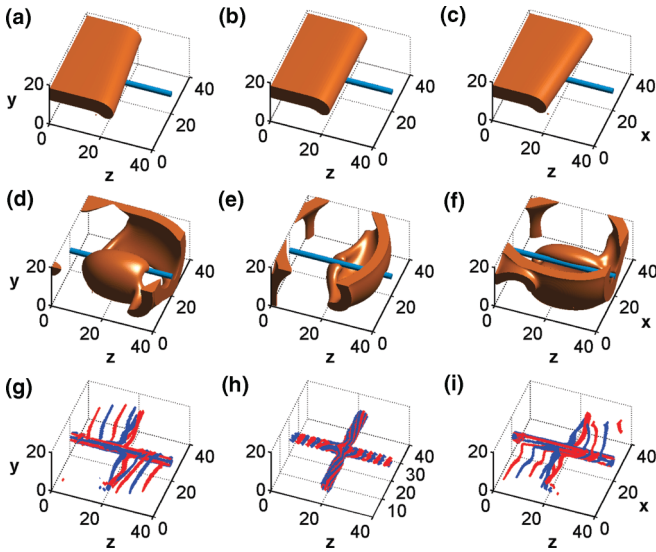
FIG. 8. (Color online) Simulated vortex dynamics for three similar initial conditions. The early filaments are nearly straight lines tilted $+5.7°$ (a), (d), (g), $0.0°$ (b), (e), (h), and $-5.7°$ (c), (f), (i) away from a line perpendicular to the pinning cylinder. The upper row shows the u pattern shortly after initiation. Solid orange areas are excited and the pinning cylinder (cyan) extends in z direction. The middle row gives the resulting wave patterns approximately 300 time units later. Notice the different rotation directions of the pinned scroll waves in (d) and (f). The corresponding filament motion is illustrated in the bottom row using alternating colors (blue and red) to help distinguish subsequent data sets.

effect could be caused by our specific choice of boundary conditions at the pinning heterogeneity.

More importantly, Figs. 8(d) and 8(e) show that the small difference in initial conditions between Figs. 8(a) and 8(c) evolve into profoundly different structures. In particular, we observe that the pinned scroll waves differ in their sense of rotation around the cylinder. This remarkable result is due to opposite drift directions of the free filament segments that extend from the cylinder to the anterior and posterior system boundaries. The underlying motion is illustrated in Figs. 8(g) and 8(i) and complemented by the stationary state [Fig. 8(h)] generated from the symmetric initial condition in Fig. 8(b).

Details concerning the dynamics of this process are presented in Fig. 9. Here we plot the distance between the filaments versus time. Following our earlier definition of contact points, the distance is computed from the z coordinates of the two filament locations that have a small distance of 2.0 from the cylinder surface. The data reveal that the small asymmetry of the initial conditions induces first slow self-wrapping in the direction favored by the tilt of the initial filament. Approximately 200 time units later, the self-wrapping speed increases smoothly to saturate at a steady speed. The symmetric initial condition in Fig. 8(b) yields no change in the filament distance.

To probe the stability of the vortex state in Fig. 8(e), we repeated the simulation with uniformly distributed noise added to the initial condition and also a more mature pattern. The temporarily perturbed states showed no indication of self-wrapping over the course of 500 time units. These findings
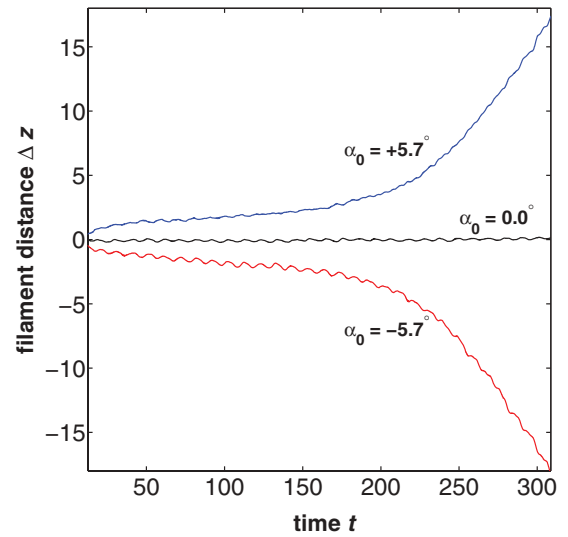

FIG. 9. (Color online) Temporal evolution of the distance Δz between the two contact points of the filaments in Fig. 8. From top to bottom the curves correspond to the initial conditions in Fig. 8(a) (blue), 8(b) (black), and 8(c) (red). The contact points are defined as the locations on the filament that have a distance of 2.0 to the surface of the pinning cylinder.

suggest that the state in Fig. 8(e) is stable and imply the existence of a low but nonzero threshold for the onset of self-pinning. Notice that such a threshold would depend in a possibly complicated fashion on the entire initial wave pattern and specifically on the initial filament. It is also reasonable to assume that the curvature-reducing motion of the free filament(s) is the primary source of the self-wrapping threshold.

The results summarized in Figs. 8 and 9 show that the direction of self-pinning is determined by the initial condition. In experiments, seemingly symmetric situations, such as the one shown in Fig. 3(a), are hence sensitive to small differences that might not be resolved in our optical data. Lastly we note that all of our experiments and simulations only employ initial conditions for which the filament and the central axis of the pinning cylinder are in the same plane. Clearly more work is needed to explore basic nonplanar cases.

VI. CONCLUSIONS

In experiments with the three-dimensional BZ reaction and numerical simulations on the basis of the Barkley model, we have shown that scroll waves self-wrap around cylindrical heterogeneities. This surprising effect stabilizes and reshapes the scroll wave. The process is most pronounced for thin cylinders and is seemingly absent for thick ones. During the self-pinning process, the free filament undergoes significant changes which involve motion along the cylinder as well as a slower rotation around the cylinder. In excitable systems with heights comparable to the vortex wavelength, these deformations can induce filament breakage at the boundaries. In larger systems, which for various technical reasons are difficult to investigate, the slow rotational motion will likely cause additional phenomena such as feedback on the self-wrapping speed and possibly highly entangled filaments. Moreover, we

found that during the self-pinning process the free part of the filament tends to be oriented nearly perpendicular to the cylinder surface. However, once the filament reaches the end of the cylinder, this angle decreases and the filament aims to depart in a tangential direction (i.e., in the direction of the cylinder axis). Our results also show that the direction of the pinning processes is selected in a way that maximizes the length of the pinned filament.

Notice that the qualitative mechanism of the self-wrapping process is not yet understood. One possible factor could be the periodic modulation of the free scroll wave by the nearby pinned vortex. In two-dimensional systems such an interaction can arise between two spiral waves either if the rotation periods are different or if one spiral arm is very short and exposes its tip to the wave field of the other vortex [38]. The three-dimensional analogs of this spiral defect drift have not been studied yet but are likely to be complex.

We believe that our findings predict profound consequences for the dynamics of scroll waves in heterogeneous media. In homogeneous media with positive filament tension, scroll waves self-annihilate or converge towards straight filaments oriented perpendicular to the system boundaries. These processes decrease the total filament length and greatly simplify the overall wave pattern. Self-pinning, on the other hand, can increase the filament length tremendously and shapes the scroll waves according to the complexities of the underlying heterogeneities. One can speculate that such patterns will show less spatiotemporal correlation and a greater persistence against external removal strategies. Such features are not only of interest from a fundamental point of view but are also relevant in cardiology where, as we mentioned before, scroll waves induce tachycardia and fibrillation.

Future studies should analyze additional configurations, such as nonplanar initial conditions and curved, tubelike heterogeneities, to expand our knowledge base regarding the self-pinning of scroll waves. Additional investigations are needed to evaluate the shape of the free filament in large systems and its effect on self-wrapping over longer distances. Of additional interest is the study of self-pinning in anisotropic systems where the self-pinning direction might be affected by the local anisotropy of the medium. We hope that our study opens up these questions for systematic investigations which eventually should yield a deeper understanding of this fascinating phenomenon and its importance in cardiology.

[1] M. C. Mackey and J. G. Milton, Ann. N.Y. Acad. Sci. **504**, 16 (1987).

[2] J. Milton and P. Jung, *Epilepsy as a Dynamic Disease* (Springer, Berlin, 2003).

[3] J. Jalife, M. Delmar, O. Anumonwo, O. Berenfeld, and J. Kalifa, *Basic Cardiac Electrophysiology for the Clinician*, 2nd ed. (Wiley-Blackwell, Oxford, UK, 2009).

[4] See, e.g., A. T. Winfree, *The Geometry of Biological Time* (Springer, New York, 1980).

[5] Y. Biton, A. Rabinovitch, D. Braunstein, M. Friedman, and I. Aviram, Phys. Lett. A **375**, 2333 (2011).

[6] J. Jalife, R. A. Gray, G. E. Morley, and J. M. Davidenko, Chaos **8**, 79 (1998).

[7] K. H. W. J. Ten Tusscher, R. Hren, and A. V. Panfilov, Circ. Res. **100**, e87 (2007).

[8] A. T. Winfree, Science **181**, 937 (1973).

[9] M. Vinson, S. Mironov, S. Mulvey, and A. Pertsov, Nature (London) **386**, 477 (1997).

[10] D. Kupitz, S. Alonso, M. Bär, and M. J. B. Hauser, Phys. Rev. E **84**, 056210 (2011).

[11] J. P. Keener and J. J. Tyson, SIAM Rev. **1**, 1 (1992).

[12] D. Margerit and D. Barkley, Chaos **12**, 636 (2002).

[13] T. Bánsági, Jr. and O. Steinbock, Phys. Rev. Lett. **97**, 198301 (2006).

[14] V. N. Biktashev, A. V. Holden, and H. Zhang, Philos. Trans. R. Soc. London A **347**, 611 (1994).

[15] S. Alonso, F. Sagués, and A. S. Mikhailov, Science **299**, 1722 (2003).

[16] F. Fenton and A. Karma, Chaos **8**, 20 (1998).

[17] F. H. Fenton, E. M. Cherry, H. M. Hastings, and S. J. Evans, Chaos **12**, 852 (2002).

[18] S. Alonso, R. Kähler, A. S. Mikhailov, and F. Sagués, Phys. Rev. E **70**, 056201 (2004).

[19] N. Wiener and A. Rosenblueth, Arch. Inst. Cardiol. Mex. **16**, 205 (1946).

[20] V. Zykov, G. Bordyugov, H. Lentz, and H. Engel, Physica D **239**, 797 (2010).

[21] O. Steinbock and S. C. Müller, Phys. Rev. E **47**, 1506 (1993).

[22] O. Steinbock and S. C. Müller, Z. Naturforsch. C **50**, 275 (1995).

[23] S. Nettesheim, A. von Oertzen, H. H. Rotermund, and G. Ertl, J. Chem. Phys. **98**, 9977 (1993).

[24] C. Cherubini, S. Filippi, and A. Gizzi, Phys. Rev. E **85**, 031915 (2012).

[25] Z. A. Jiménez, B. Marts, and O. Steinbock, Phys. Rev. Lett. **102**, 244101 (2009).

[26] Z. A. Jiménez and O. Steinbock, Europhys. Lett. **91**, 50002 (2010).

[27] S. Dutta and O. Steinbock, J. Phys. Chem. Lett. **2**, 945 (2011).

[28] Z. A. Jiménez and O. Steinbock, Phys. Rev. Lett. **109**, 098301 (2012).

[29] B. Marts, T. Bánsági, Jr., and O. Steinbock, Europhys. Lett. **83**, 30010 (2008).

[30] A. M. Pertsov, M. Wellner, M. Vinson, and J. Jalife, Phys. Rev. Lett. **84**, 2738 (2000).

[31] E. Vigmond, F. Vadakkumpadan, V. Gurev, H. Arevalo, M. Deo, G. Plank, and N. Trayanova, Exp. Physiol. **94**, 563 (2009).

[32] A. Arenal, J. Hernández, E. Pérez-David, J. L. Rubio-Guivernau, M. J. Ledesma-Carbayo, and F. Fernández-Avilés, Cardiovascular Res. **94**, 324 (2012).

[33] S. Luther *et al.*, Nature (London) **475**, 235 (2011).

[34] T. Bánsági, Jr., V. K. Vanag, and I. R. Epstein, Science **331**, 1309 (2011).

[35] See Supplemental Material at http://link.aps.org/supplemental/10.1103/PhysRevE.86.036205 for a schematic view of the experimental procedure and for a scroll ring pinned to two cylinders of larger radii.

[36] D. Barkley, Physica D **49**, 61 (1991).

[37] M. Dowle, R. M. Mantel, and D. Barkley, Int. J. Bifurcat. Chaos **7**, 2529 (1997).

[38] S. Dutta and O. Steinbock, Phys. Rev. E **83**, 056213 (2011).